ROSAT PSPC OBSERVATIONS OF TWO X-RAY–FAINT EARLY-TYPE GALAXIES: NGC 4365 AND NGC 4382

G. FABBIANO

Harvard-Smithsonian Center for Astrophysics, 60 Garden Street, Cambridge, MA 02138

D.-W. KIM

Chungnam National University, Daejeon 305-764, South Korea, and Harvard-Smithsonian Center for Astrophysics

AND

G. TRINCHIERI

Osservatorio Astrofisico di Brera, Via Brera 28, Milano 20121, Italy, and Harvard-Smithsonian Center for Astrophysics

ABSTRACT

We present the results of *ROSAT* PSPC observations of the two early-type galaxies NGC 4365 and NGC 4382. These galaxies are among those observed with *Einstein* to have the lowest X-ray to optical flux ratios of early-type galaxies. The PSPC data show that for radii $r > 50''$ the radial distributions of the X-ray surface brightness are consistent with the optical distributions of King (1978). We also find that these galaxies have X-ray spectra significantly different from those observed in X-ray–bright ellipticals, with a relative excess of counts detected in the softest spectral channels. This confirms earlier *Einstein* results. The characteristics of the *ROSAT* PSPC do not allow us to discriminate between possible spectral models. If we adopt a two-component thermal model on the grounds of physical plausibility, we find that the spectral data can be fitted with a very soft optically thin component, with $kT \sim 0.2$ keV, and a hard component with $kT > (1.0–1.5)$ keV. The hard component has a luminosity consistent with that expected from the integrated emission of a population of low-mass X-ray binaries in these galaxies; the nature of the very soft component is more speculative. Candidates include the coronal emission of late-type stars, supersoft X-ray sources, RS CVn, and perhaps a hot ISM. Alternatively, the spectral data may be fitted with a 0.6–1 keV bremsstrahlung spectrum (exponential plus Gaunt), and may suggest the presence of a totally new population of X-ray sources.

Subject headings: galaxies: elliptical and lenticular, cD — galaxies: individual (NGC 4365, NGC 4382) — radiation mechanisms: nonthermal — radiation mechanisms: thermal — X-rays: galaxies

1. INTRODUCTION

Observations of early-type galaxies with the *Einstein* satellite (Giacconi et al. 1979) have revealed that these galaxies can retain large amounts (up to $\sim 10^{11}$ $M_\odot$) of hot ($T \sim 10^7$ K) interstellar medium (ISM; Forman, Jones, & Tucker 1985; Canizares, Fabbiano, & Trinchieri 1987). However, it was also observed that early-type galaxies of the same optical luminosity can have X-ray luminosities differing up to a factor of ~ 100 (e.g., Fabbiano, Kim, & Trinchieri 1992). While there are convincing observational and theoretical arguments suggesting that the X-ray emission of X-ray bright galaxies is dominated by the hot ISM, the origin of the emission of X-ray faint galaxies is less certain (Canizares et al. 1987; Fabbiano, Gioia, & Trinchieri 1989; see Fabbiano 1989 and references therein). These galaxies may have not been able to retain their hot ISM, which may have been either expelled through winds (e.g., Ciotti et al. 1991; David, Freeman, & Jones 1991) or stripped through interaction with a hot Intracluster Medium (e.g., White & Sarazin 1991).

A recent analysis of the *Einstein* IPC data of elliptical galaxies in different ranges of X-ray to optical ratio (L_X/L_B) has shown significant differences in the average spectral properties of the X-ray emission (Kim, Fabbiano, & Trinchieri 1992b), which may support these conclusions. While X-ray bright galaxies [log $(L_X/L_B) > 30.3$, where L_X/L_B is in ergs s$^{-1}/L_\odot^{-1}$] have average spectra that can be fitted with thermal Raymond models with $kT \sim 1$ keV, with decreasing L_X/L_B the spectra become virtually indistinguishable from those of spiral gal-

axies, which are significantly harder ($kT > 3$ keV), and whose emission is dominated by populations of evolved X-ray sources (see Fabbiano 1989). However, an unexpected very soft component of the X-ray emission is apparent in the average X-ray spectrum of the X-ray faintest galaxies [Group 1 in Kim et al. 1992b; log $(L_X/L_B) = 29.3–30.0$] as a significant excess of counts in the lowest spectral channels.

To confirm the existence of this very soft emission in X-ray faint early-type galaxies, and to determine its characteristics, we have observed two of these galaxies, NGC 4365 and NGC 4382, with the *ROSAT* (Trümper 1983) PSPC (Pfeffermann et al. 1987). In this paper, we report the results of these observations, and we discuss briefly their implications. In the companion paper (Pellegrini & Fabbiano 1994), these results are compared with detailed model predictions.

2. OBSERVATIONS, DATA ANALYSIS AND RESULTS

Table 1 summarizes the characteristics of our two X-ray faint galaxies and gives the *ROSAT* PSPC observation log.

2.1. *Contour Plots*

The data were analyzed using the "xray" package of IRAF, developed at SAO for the analysis of X-ray data. Figures 1a and 1b show contours plots of the central parts of the two PSPC images, containing the target galaxies. Data from spectral channels 7 to 240 were used. The PSPC data were binned in 5'' pixels and smoothed with 15'' Gaussians to obtain these plots. As it is readily visible from Figure 1, extended X-ray

TABLE 1

GALAXY AND OBSERVATION PARAMETERS

Name (NGC)	Type	R.A., Decl. (B1950)	R.A., Decl. (J2000)	D (Mpc)	N_H[a] (cm^{-2})	L_X[b] (*Einstein*)	$\log L_X/L_B$[c] (*Einstein*)	PSPC Start/Stop	On-time (s)
4365........	−5 E	$12^h21^m56^s +07°35'42''$	$12^h24^m29^s +07°19'05''$	27	1.6×10^{20}	$2.6 \pm 0.4 \times 10^{40}$	29.61	91 Dec 15 91 Dec 16	14904
4382........	−2 S0	12 22 53 +18 28 00	12 25 25 +18 11 25	27	2.7×10^{20}	$5.2 \pm 0.4 \times 10^{40}$	29.71	91 Dec 14 91 Dec 24	8632

[a] From Stark et al.

[b] L_X(0.2–4.0 keV) is in units of ergs s^{-1} and assumes a $kT = 1$ keV Raymond spectrum with solar abundances (Fabbiano, Kim, & Trinchieri 1992). Errors are statistical only.

[c] L_X/L_B is in units of ergs s^{-1} $L_\odot^{-1}$ (see Kim, Fabbiano, & Trinchieri 1992b).

sources were detected in both cases, associated with the two galaxies. Other serendipitous sources are visible in the two fields. A comparison between the isophotes of pointlike seren-dipitous sources, and those of the emission associated with the two galaxies, demonstrates qualitatively that the latter are not pointlike. The emission of these galaxies could not be resolved with the *Einstein* IPC (see Fabbiano et al. 1992). In both cases the isophotes are well within the optical extent of the galaxies. The surface brightness distribution of NGC 4365 shows some azimuthal variations (see also § 2.5). The surface brightness of NGC 4382 is more circularly symmetric, except for an elon-gation toward the south, which cannot be resolved as a separate emission region with the PSPC.

In NGC 4382 we resolve a pointlike source at the N-W of the extended emission. This source was not resolved with the *Einstein* IPC, although the *Einstein* isophotes show a slight extension in this direction (Fabbiano et al. 1992). This source contributes ~74 counts to the image, and it would have an X-ray luminosity near 10^{40} ergs s^{-1} were it at the distance of NGC 4382 (using the parameters of Table 4 below). This lumi-nosity would be exceptionally high for a single low-mass X-ray binary of the type that might be expected in an early-type galaxy (see Fabbiano 1989, and references therein). However, it is possible that we are dealing with an interloper, and to be conservative we will treat it as such.

2.2. *Background Subtraction and Extraction of Source Counts and Exposure Times*

To extract counts for flux determination and for spectral analysis, and to study the radial behavior of the X-ray surface brightness, the field background must be subtracted from the images. To this end, we have followed a method similar to that adopted by Fabbiano et al. (1992) for the analysis of *Einstein* IPC images of galaxies. Using the broad-band images provided by the *ROSAT* pipeline processing, we have first subtracted all strong point sources detected in the fields, by excluding circu-lar areas centered on these sources. These were determined both by inspection of the results of the pipeline processing of the data, which provides a list of sources, and by visual inspec-tion of the data with the SAO image tool. This done, radial profiles of the two fields were obtained, by binning the data around the centroids of the galaxy emission. These radial pro-files were then compared with similarly binned profiles of the field background, provided by the pipeline processing. The case of NGC 4365 is shown in Figure 2. For both observations it was evident that the radial profiles of the galaxy images flattened to a constant level at radii between 5' and 10', in a region when mirror vignetting effects are minor. That this is the case is shown quite clearly by the flatness of the field back-ground at these radii. Because of this relatively small source
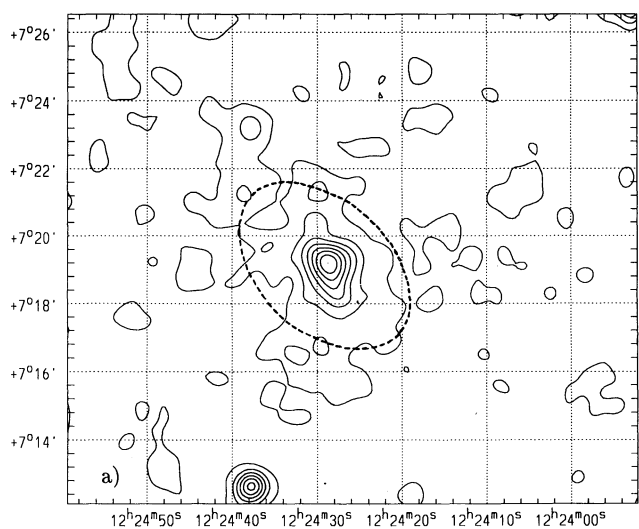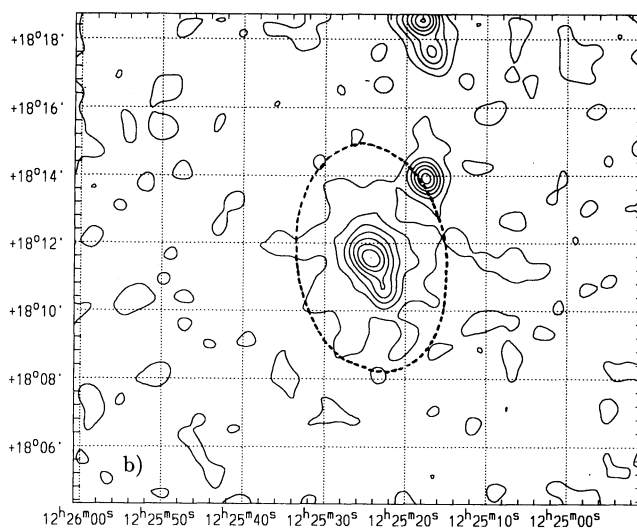

FIG. 1.—Contour plots of the X-ray emission of NGC 4365 (*a*) and NGC 4382 (*b*). In both cases data from spectral channels 7–240 (~0.1–2.0 keV) were used. Data were binned in 5" pixels and smoothed with 15" Gaussians. Contour plotted are linearly spaced from 4% to 100% of peak in (*a*), and from 5% to 100% of peak in (*b*). The ellipses indicate the optical galaxies. Coordinates are J2000.
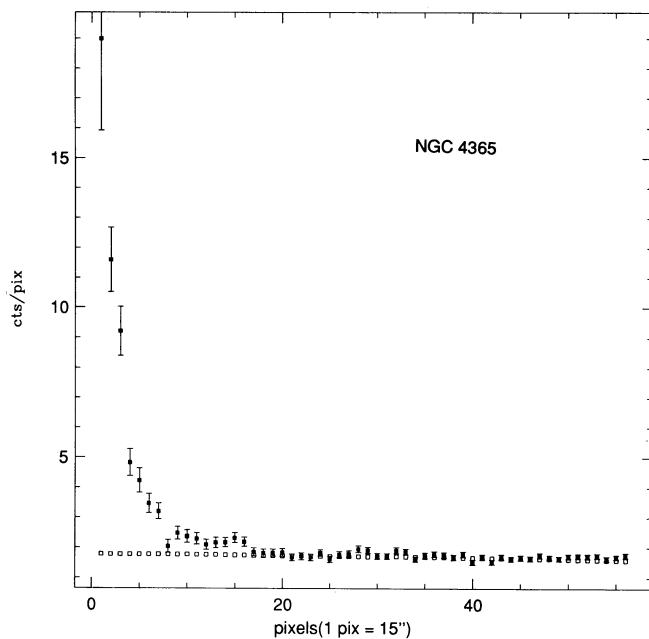
FIG. 2.—Radial distribution of surface brightness in the central part of the NGC 4365 field after subtraction of other sources in the field, compared with the radial distribution of the background map.

have estimated the average exposure time in the area used for source count extraction. We have also included an instrument dead-time correction of 97%. These times are given in Table 2.

2.3. *Surface Brightness Profiles*

We produced surface brightness profiles of the two galaxies, by binning the data in concentric 30″ annuli centered on the peaks of the surface brightness distributions, determined with the aid of isointensity contour maps (see Fig. 1 and Table 2). The background was subtracted, as described above. We used only data from Pulse Invariant (PI) gain-corrected spectral channel 26-247 (0.27–2.48 keV), because "ghost images" cause a spurious flattening of the profile at the lower energies. This is an instrumental effect, that "spreads out" soft photons (PI < 25) between sets of adjacent PSPC cross-wires (Hasinger et al. 1992). In Figure 3 we show the (PI 26-247) profiles for both galaxies. The source at the N-W of NGC 4382 (see Fig. 1b) is not included in the surface brightness profile of this galaxy. In Figure 3a we also plot a representation of the *ROSAT* PSPC Point Response Function (Hasinger et al. 1992). It is obvious that the galaxy emission is significantly extended in both cases.

The optical surface brightness profiles of King (1978) were renormalized to make them fit the X-ray profiles and plotted in Figure 3 as solid lines. The X-ray surface brightness profiles are consistent with the optical ones, with the exception of the innermost X-ray point which falls well below the optical profile. This is where the PSPC PSF would flatten the X-ray profile. At least for NGC 4365 a simple convolution of the King (1978) profile with the PSPC PSF suggests that the X-ray profile might still be somewhat relatively depressed at the center (see the companion paper, Pellegrini & Fabbiano 1994). However, the discrepancy is such that could be explained away with uncertainties on the assumed PSPC PSF. A detailed comparison over a large range of radii is necessary for discriminating between different options on the nature of the X-ray emission (see § 3, and Pellegrini & Fabbiano 1994). A further complication in these comparisons derives from azimuthal asymmetries in the surface brightness distributions of both galaxies (see Fig. 1). In NGC 4365, which was detected with a higher signal-to-noise ratio, we find that the profile in 135–225 deg azimuthal pie declines less rapidly than the profiles from other aximuthal sectors between 40″–80″ (Fig. 4). However, with the present data we cannot comment further on the nature of these asymmetries, and on the possible presence of background or foreground sources, superposed on the galaxy extended emission. The best way to proceed is to obtain high resolution HRI data. HRI observations would allow us to follow the X-ray

extent, we derived the background locally in both cases, by using annuli surrounding the galaxy emission, from which we have excluded areas containing other sources. In the case of NGC 4382 (see § 2.1), there is a point source to the N-W of the extended emission, which falls within the optical extent of the galaxy. We give source counts with and without this source. The parameters used for count extraction and the results are summarized in Table 2. This procedure resulted in 855.0 ± 54.0 counts detected in NGC 4365, and 507.0 ± 34.1 counts detected in NGC 4382 (without N-W point source) between 0.1 and 2.0 keV.

To calculate count rates, we also need to estimate the average exposure time in the region of interest. Because of local variations in the quantum efficiency of the PSPC, of vignetting, and the presence of the support structure (both ribs and wire mesh), the effective exposure time is a function of the position of the source in the instrumental field. At the center of the field, the exposure time is typically within ±2% of the instrument on-time (the time during which the data included in the image were collected). The instrumental effects that affect the effective exposure on the source are included in the exposure map, provided with the data package. By using the exposure map, we

TABLE 2

SOURCE COUNT AND EXPOSURE TIME EXTRACTION

Galaxy (NGC)	Source[a] (x, y; radius)	Background[a] (x, y; radii)	Excluded[a] (x, y; radius)	Net Counts (0.1–2.0 keV)	Exposure Time (s)	Rate (counts s^{-1})
4365.........	7630, 7680; 250	7630, 7680; 300–500	7350, 6870; 110	855.0 ± 54.0	14429	0.06
4382.........	7750, 7700; 220	7750, 7700; 300–500	7000, 8290; 90	507.0 ± 34.1[b]	8320	0.06
			7930, 8510; 90	581.3 ± 36.0[c]		
			7960, 7970; 60			
			8270, 7330; 90			

[a] x and y are in instrument pixels; radii are in arcsec.
[b] Excluding the source at 7960, 7970.
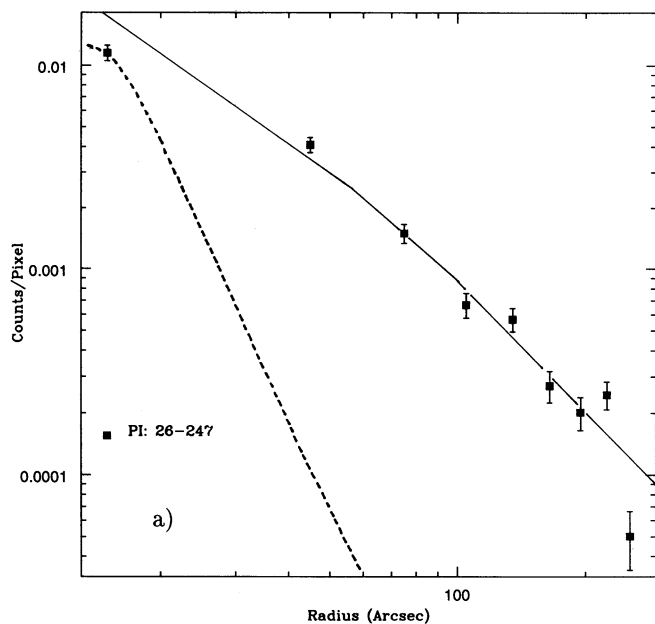[c] Including the source at 7960, 7970.
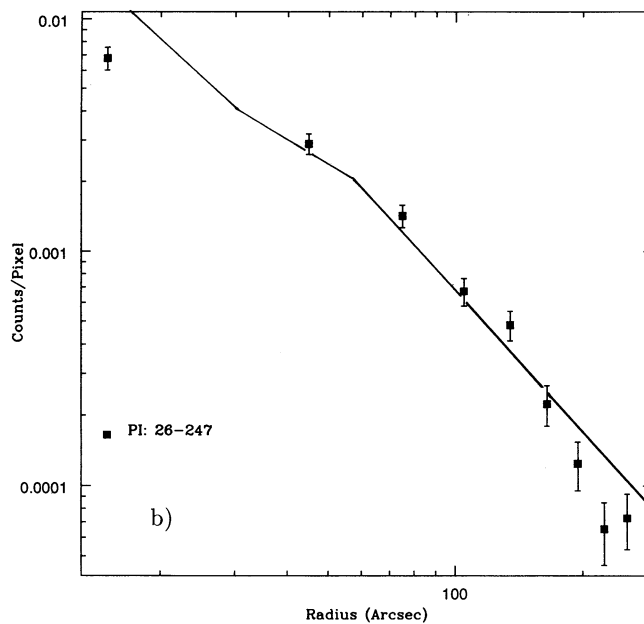
Fig. 3a

Fig. 3b

Fig. 3.—Radial surface brightness profiles of NGC 4365 (*a*) and NGC 4382 (*b*); see text for details. The dashed line approximates the PSPC PRF. The solid lines represent the optical surface brightness profile of King (1978), arbitrarily renormalized.

surface brightness distribution down to radii comparable to those of average seeing ground-based optical data, and would resolve out significantly bright interlopers. We plan to pursue this point with future *ROSAT* observing programs.

2.4. *Spectral Analysis*

Counts for spectral analysis were extracted from the regions defined in § 2.2 above. We fitted the data to different models using both the IRAF/xray spectral routines and XSPEC (provided by the NASA HEASARC). The spectral fit program

Fig. 4.—Azimuthal asymmetries in the X-ray radial surface brightness profile of NGC 4365. The solid line represents the optical profile (King 1978).

in IRAF/xray rebins the spectral data (originally in 256 PI bins) into 34 bins, covering an energy range of 0.07 to 2.48 keV. These data are then compared via χ^2 fits to models, convolved with the instrument and mirror response. We have excluded from the fits spectral bins with fewer than ~ 10 counts at the upper end of the *ROSAT* spectral range (see Table 3), because the software use a Gaussian approximation to calculate statistical uncertainties. We have also excluded the two lower spectral bins and the C-edge data, because the response function of the PSPC is less well determined in these regions (Hasinger et al. 1992). In all cases, these points turn out to be consistent with our best-fit predictions.

Since the emission is clearly extended (§§ 2.1 and 2.3), we did not attempt to fit our data to power-law models, which have been used to describe the X-ray spectra of AGNs. We used instead models that have been used to describe the *Einstein* spectral data of galaxies (see Kim et al. 1992a, b). These are Raymond models (see Raymond & Smith 1977), which describe the thermal emission of an optically thin gas of a given temperature and chemical composition, and include continuum and line contributions; and the bremsstrahlung model, approximated as an exponential with Gaunt factor. In the absence of metals (pure hydrogen gas), the line contribution is of course suppressed from the Raymond models, which are then approximated with exponential plus Gaunt models. In all cases, we add an absorption term at the low energies, to model the absorption of X-ray photons by intervening cold interstellar medium, using the Morrison-McCammon (1983) cross sections.

Raymond models are a reasonable first step for modeling the emission of a hot ISM ($kT \sim 1$ keV), such as has been detected in X-ray bright ellipticals (see Fabbiano 1989; Serlemitsos et al. 1994). Bremsstrahlung emission with higher emission temperatures ($kT > 5$ keV) has been used to fit the emission of binary X-ray sources (e.g., Jones 1977), although more complex models are suggested by more recent higher quality spectral
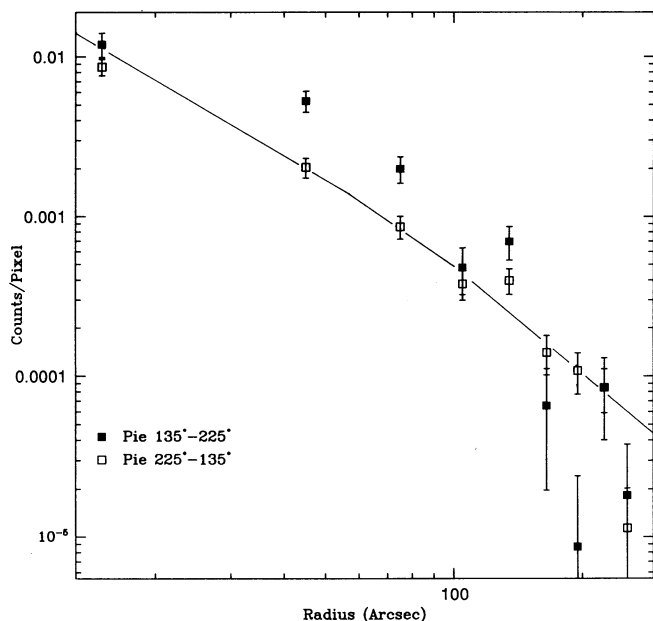
observations (e.g., Makishima & Mitsuda 1985). Bremmstrahlung models have been used to describe the spectra of spiral galaxies, where the emission is likely to be dominated by a population of X-ray binaries (see Fabbiano 1989; Kim et al. 1992a, b). A population of low-mass binaries is responsible for the X-ray emission of the bulge of M31 (Fabbiano, Trinchieri, & Van Speybroeck 1987), and a similar component is likely to be present as baseline emission in elliptical and S0 galaxies (Trinchieri & Fabbiano 1985; Canizares et al. 1987; see Fabbiano 1989). With the *Einstein* data, it was impossible to choose between Raymond and bremsstrahlung models on the basis of goodness of fit; however for both models there were definite trends in the emission temperature with galaxy morphology, or in the case of ellipticals, with L_X/L_B (see Kim et al. 1992a, b). With good signal to noise *ROSAT* PSPC data, it is clear that a Raymond model describes well the data of X-ray bright ellipticals (e.g., NGC 4636, Trinchieri et al. 1994), while a simple bremsstrahlung model cannot account for the emission near 1 keV, which is dominated by the line contribution.

The data used for the fits and the best-fit parameters are summarized in Table 3. We used the 1993 January spectral matrix to derive these values. Using the 1992 March response matrix does not affect our results (within the error range), because our uncertainties are dominated by statistics.

2.4.1. NGC 4365

Our first attempt was to fit the data with one-temperature optically thin Raymond models with solar abundances and line of sight absorption, calculated using the Morrison-McCammon (1983) cross sections. For this purpose we used the latest Raymond tables available (J. Raymond 1992, private communication), which are included in the IRAF/xray package. We find that the best-fit χ^2 is unacceptable (see Table 3). The spectral counts, compared with the best-fit spectrum are shown in Figure 5a. A very significant improvement in the fit is found when a two-temperature model is used. The F-test gives a probability $P \ll 10^{-2}$ of exceeding F for two additional parameters. The best-fit spectrum and the two spectral components are compared with the data in Figure 5b. The fit does not improve when a third component is added. Note that adopting a model with a low-temperature Raymond component and a high-temperature bremsstrahlung emission we obtain basically the same results. This is because a high-temperature Raymond spectrum has relatively weak emission lines and (with the *ROSAT* PSPC resolution) cannot be distinguished from pure continuum emission.

The best-fit parameters quoted in Table 3 were derived restricting the absorption column to be greater than 10^{20} cm^{-2}, consistent with the line-of-sight neutral hydrogen column (see Table 1). However, if N_H is unrestricted the best-fit

N_H tends to be lower than the line-of-sight H I values, but the change in χ^2 is small. The parameter kT_2 was restricted to vary within 3 keV, because of the lack of spectral response above 2.5 keV. Using the confidence contours for the *two* interesting parameters kT_1 and kT_2 (the temperatures of the two components) we find that the temperature of the soft component (kT_1) has well-determined values between 0.15 and 0.26 keV (at 90% confidence); the temperature of the hard component (kT_2) is less well defined, because of the spectral response of the PSPC, but values of $kT_2 < 1.5$ keV are excluded. These contours were derived for log $N_H = 20.0$, which is near the line-of-sight value, leaving all other parameters free to vary. However, if log N_H is allowed to be as low as 19.0, kT_1 may assume higher values (0.2–0.4 keV at 90% confidence). In this case, the preferred values of log N_H is 19.0. However, as said above, the improvement in the value of χ^2 is relatively small.

Assuming that N_H is only line of sight (and solar abundances), the spectral shape is completely defined by three parameters: kT_1, kT_2, and the ratio of the normalizations of the two components. In Figure 6, we show the 68%, 90%, and 99% confidence contours for these *three* interesting parameters. (Note: all of the above reported values of confidence intervals were derived with IRAF/xray; using XSPEC we find lower limits on kT_2—near 1 keV—both for NGC 4365 and NGC 4382, which is discussed below.)

We attempted to fit the data with element abundances other than solar, but we did not find significant differences in our results for the range of abundances allowed by the IRAF/xray software. Lower values of abundance ($\sim 10\%$ solar) tend to give more realistic values of the best-fit N_H, compatible with the line-of-sight value. However, the difference in χ^2 is very small. XSPEC allows more flexibility in varying the abundance. With XSPEC we found that a one-temperature model, with line of sight N_H gives a good fit to the data, for abundance values close to zero ($<4\%$ solar at 90% confidence for two interesting parameters, abundance and kT). In this case the temperature is between 0.6 and 1.1 keV (at 90% confidence) and the best-fit χ^2 is 25.4 for 19 degrees of freedom. Not surprisingly, a single bremsstrahlung component gives a similar good fit to the data, with similar parameters.

Unfortunately, with the limited bandwidth and spectral resolution of the *ROSAT* data we cannot distinguish between the two-temperature model, and the zero metal abundance model (or bremsstrahlung) on the basis of the data alone. Other considerations will have to enter in our choice of model (see § 3).

We searched for radial variations in the spectral parameters, by analyzing separately data from concentric annuli of increasing radii. No significant differences were found, except a pos-

TABLE 3

SPECTRAL ANALYSIS: COUNT EXTRACTION AND BEST-FIT VALUES

GALAXY (NGC)	BINS	ENERGY (keV)	COUNTS ± ERROR	ONE-TEMPERATURE RAYMOND				TWO-TEMPERATURE RAYMOND				
				log N_H(cm^{-2})	kT(keV)	χ^2	ν	log N_H(cm^{-2})	kT_1(keV)	kT_2(keV)	χ^2	ν
4365.........	3–11	0.11–0.47	812.18 ± 52.91	20.0	3.0	63.2	19	20.0	0.20 (0.15–0.26)[a]	3.0 (>1.5)[a]	24.3	17
	13–25	0.52–1.50										
4382.........	3–10	0.11–0.42	463.50 ± 32.66	20.0	3.0	57.1	17	20.1	0.24 (0.18–0.31)[a]	3.0 (>1.2)[a]	14.3	15
	13–24	0.52–1.41										

[a] These are the 90% confidence intervals for two interesting parameters estimated using the IRAF/xray software; with EXSPEC we find lower limits near 1 keV (see text).
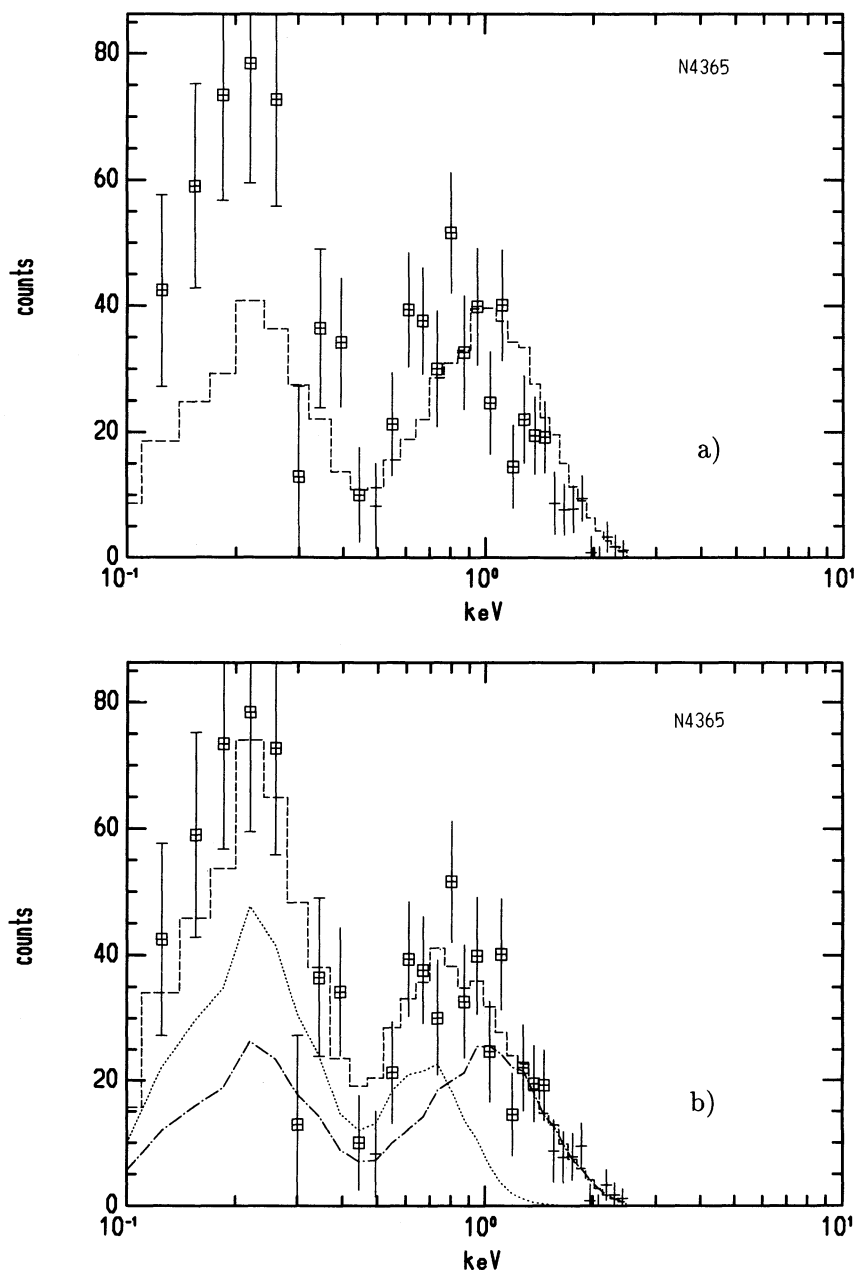
Fig. 5.—Comparison of the observed distribution of the PSPC spectral counts of NGC 4365 with (*a*) one-temperature best-fit; (*b*) two-temperatures best-fit. Both two-component spectrum and each individual component are plotted.

sible softening of the spectrum at the outer radii (120″–250″). However, this result is likely to be due to an instrumental effect, that "spreads out" soft photons ($PI < 25$) between sets of adjacent PSPC cross-wires ("ghost images," Hasinger et al. 1992).

2.4.2. *NGC 4382*

Similar results were found in the analysis of the spectral data of NGC 4382. The single component fit with solar abundance is unacceptable, while adding a second thermal component we find a good fit (Table 3, Fig. 7). The improvement in χ^2 is highly significant. As in the case of NGC 4365, the low-temperature component is well defined (kT_1 between 0.18 and 0.31 at 90% confidence for the *two* interesting parameters kT_1

and kT_2); the values of the high-temperature component are less well defined, because of the fewer detected counts. Nonetheless, values of $kT_2 < 1.2$ keV are excluded (at 90% confidence). The confidence contours for the *three* interesting parameters, kT_1, kT_2, and ratio of hard/soft normalizations are shown in Figure 8. Notice that these confidence regions are less well defined than those of NGC 4365, reflecting the smaller statistical significance of the NGC 4382 data.

As for NGC 4365, we find that the data are also well fitted with a one-temperature Raymond model with very low metal abundances and line-of-sight N_H (minimum $\chi^2 = 17.8$ for $v = 16$ degrees of freedom). However, in this case the allowed parameter space is less extreme, reflecting the poorer counting statistics. We find a best fit abundance of 2% solar ($< 20\%$
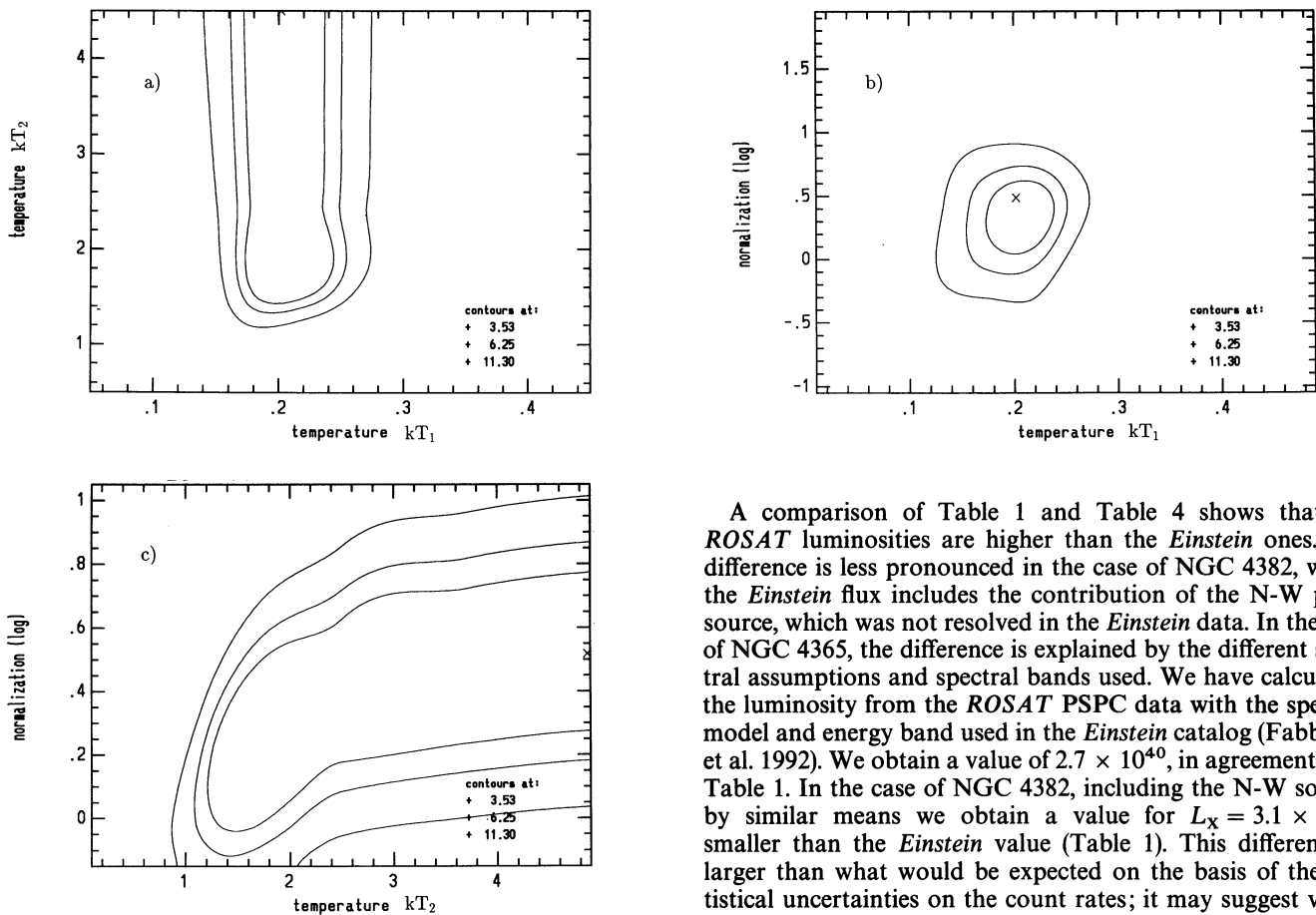
FIG. 6.—χ^2 confidence contours for the three interesting parameters, two temperatures and normalization of the hard component relative to that of the soft component for NGC 4365. The temperatures are in keV and the ratio of normalizations (hard/soft) is in log units. (a) The two temperatures; (b) the temperature of the soft component (kT_1) and the ratio of normalizations; (c) the temperature of the hard component (kT_2) and the ratio of normalizations.

solar at 90% confidence for two interesting parameters abundance and kT), and $kT = 0.30-0.65$ keV (at 90%).

2.5. *Fluxes and Luminosities*

Table 4 gives fluxes and luminosities in the 0.1–2.0 keV range for the entire detected emission, using the best-fit two-component spectra, and for the soft and hard best-fit components separately. To obtain a rough measure of the uncertainty in the fluxes due to the uncertainties of the normalization of the spectral components, we have kept the temperatures of the two components fixed at 0.2 and 3.0 keV, respectively, and we have used different sets of normalizations, to achieve an increase in χ^2 of ~ 10. This would correspond to a 99% confidence interval on the normalization (two interesting parameters). We find that the relative fluxes of the two components, which are comparable in the best-fit case, can vary up to a factor of 2 in each direction in NGC 4365. A similar exercise for NGC 4382 shows a similar uncertainty for the soft component. The luminosity of the hard component could vary upward of up to a factor of 3. If we consider the full allowed range of parameters (Figs. 6 and 8), then the flux of the hard component could range from $\sim 80\%$ to ~ 6 times that of the soft component in NGC 4365, and from $\sim 30\%$ to 3 times, in NGC 4382.

A comparison of Table 1 and Table 4 shows that the *ROSAT* luminosities are higher than the *Einstein* ones. The difference is less pronounced in the case of NGC 4382, where the *Einstein* flux includes the contribution of the N-W point source, which was not resolved in the *Einstein* data. In the case of NGC 4365, the difference is explained by the different spectral assumptions and spectral bands used. We have calculated the luminosity from the *ROSAT* PSPC data with the spectral model and energy band used in the *Einstein* catalog (Fabbiano et al. 1992). We obtain a value of 2.7×10^{40}, in agreement with Table 1. In the case of NGC 4382, including the N-W source, by similar means we obtain a value for $L_X = 3.1 \times 10^{40}$, smaller than the *Einstein* value (Table 1). This difference is larger than what would be expected on the basis of the statistical uncertainties on the count rates; it may suggest variability of the N-W source.

3. DISCUSSION

3.1. *Multicomponent Emission?*

The *ROSAT* PSPC observations of the two X-ray faint ellipticals NGC 4365 and NGC 4382 confirm the presence of significant emission in the very soft spectral channels, that was suggested by the *Einstein* IPC data (Kim et al. 1992b). This type of spectral distribution is very different from that of X-ray bright ellipticals, where most of the spectral counts are instead observed around 1 keV. The difference is immediate when comparing Figures 5 and 7 with the PSPC spectral distribution of the X-ray bright NGC 4636 (Fig. 9, reproduced from Trinchieri et al. 1994; see also Fabbiano 1993). For this galaxy there is no doubt that the data require a line emission component peaking around 1 keV, making a strong case for the presence of a hot (~ 0.8 keV) ISM (see Trinchieri et al. 1994).

The *ROSAT* passband and spectral resolution are such that a unique spectral model cannot be found to describe our data. A single temperature optically thin spectrum with solar (or a significant fraction of solar) abundances and line of sight absorption is excluded in our case. However, both a two-temperature model with abundances ranging from solar down to $\sim 10\%$ solar, and a single temperature model with less than 4% solar abundance give acceptable fits to the data of NGC 4365. In the case of NGC 4382, both two-temperature and one-temperature low-abundance models fit the data well, but the constraints are less extreme because of the poorer counting statistics.

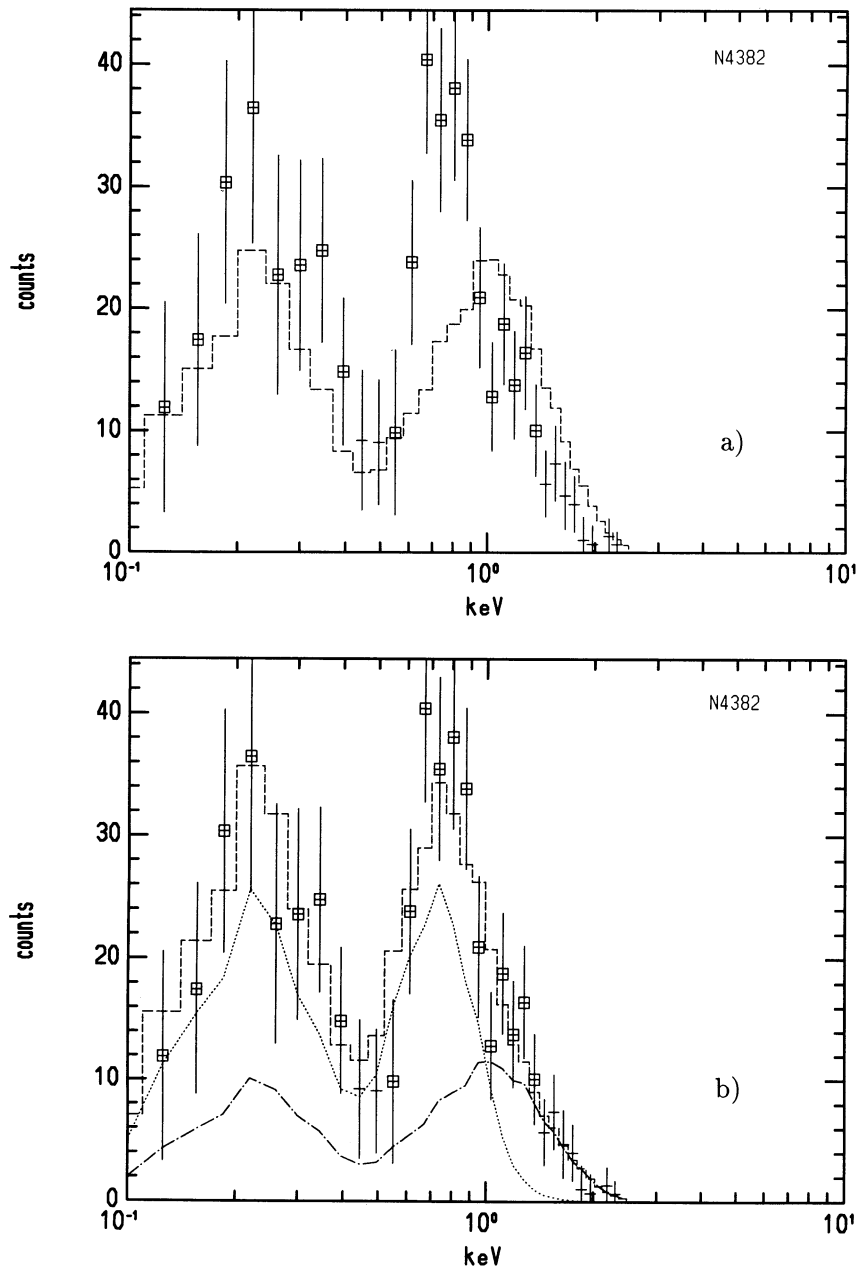Although the ultimate solution of this puzzle requires

FIG. 7.—Comparison of the observed distribution of the PSPC spectral counts of NGC 4382 with (*a*) one-temperature best-fit; (*b*) two-temperatures best-fit

obtaining higher resolution spectral data on a wider spectral band, such as the ASCA satellite may provide, at this point we are inclined to consider the two-temperature model to be the more realistic option. Our reasons are discussed in detail below.

A close to zero metal abundance, as required by the fit to the NGC 4365 data, is unphysical if the emission is due to a hot (~0.8 keV) ISM. Lower than solar metallicities have been reported from X-ray observations of early-type galaxies (e.g., Serlemitsos et al. 1994), but not at these low values. Unless the thermally emitting medium is primordial metal-free material suddenly accreted by a galaxy that has been swept clean of its own ISM, metal enrichment from Type Ia supernovae (SN Ia) and stellar winds has to be expected (e.g., Renzini et al. 1993). In the zero abundance model, of the order 10^8 $M_\odot$ of hot gas

would be needed to explain the observed flux (see Trinchieri, Fabbiano, & Canizares 1986). Only 10^7 $M_\odot$ of wind from the evolving stars would be needed to pollute a metal free medium to ~10% solar abundances (assuming solar abundances for the stars). Given a crossing time of ~10^8 years and a mass loss rate of ~1 $M_\odot$ year^{-1}, it will take only 0.1 crossing times to achieve a 10% solar enrichment. Moreover, NGC 4365 has a counter-rotating core, suggesting that it is the product of a merger (Surma 1993). In this case, we would expect some enrichment in the ISM of the parent galaxies, and of the merger remnant itself, if the merger triggers a burst of star formation (Surma 1993; Schweizer 1993).

Another possible explanation for the single component fit is that the emission is not from an optically thin gas devoid of metals, but that is due to a population of sources whose spec-
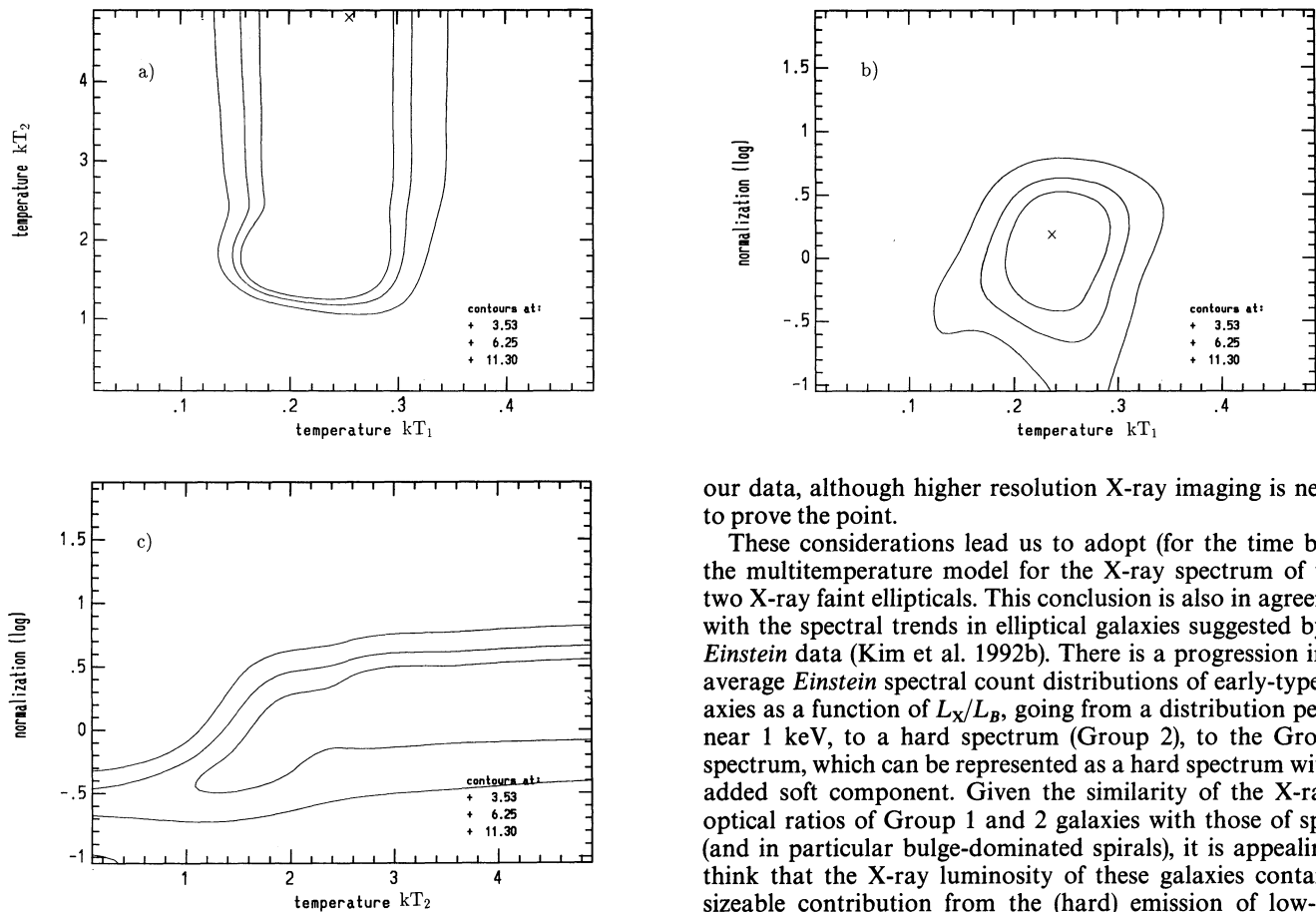
FIG. 8.—Same as Fig. 6, but for NGC 4382.

trum can be modeled with an average $kT \sim 0.6$–1. keV bremsstrahlung emission. The following considerations lead us to rate this option as less plausible. The old stellar population of these galaxies suggests that such sources (if present) ought to be low-mass binary systems. Stellar coronal emission would have typically lower emission temperatures (see Vaiana 1990), and supernova remnants are not likely to be a relevant component in early-type galaxies. However, Galactic data and *Einstein* observations of the bulge of M31 (Fabbiano et al. 1987, and references therein) show that low-mass binaries have higher kT, when modeled with bremsstralung emission. Therefore, in this hypothesis, one must postulate the existence of an entirely new population of X-ray sources. In this hypothesis, the X-ray and optical surface brightness profiles should follow each other. As discussed in § 2.3, this cannot be excluded with

our data, although higher resolution X-ray imaging is needed to prove the point.

These considerations lead us to adopt (for the time being) the multitemperature model for the X-ray spectrum of these two X-ray faint ellipticals. This conclusion is also in agreement with the spectral trends in elliptical galaxies suggested by the *Einstein* data (Kim et al. 1992b). There is a progression in the average *Einstein* spectral count distributions of early-type galaxies as a function of L_X/L_B, going from a distribution peaked near 1 keV, to a hard spectrum (Group 2), to the Group 1 spectrum, which can be represented as a hard spectrum with an added soft component. Given the similarity of the X-ray to optical ratios of Group 1 and 2 galaxies with those of spirals (and in particular bulge-dominated spirals), it is appealing to think that the X-ray luminosity of these galaxies contains a sizeable contribution from the (hard) emission of low-mass binaries (see also Fabbiano 1989; Fabbiano et al. 1989; Canizares et al. 1987; Fabbiano et al. 1987; Trinchieri & Fabbiano 1985). The hard spectral distribution of Group 2 galaxies suggests that this baseline component is starting to appear, and in the two-temperature model it would also be present in the spectra of the yet X-ray fainter Group 1 galaxies, to whom our two galaxies belong.

3.2. *The Hard Component*

In the two-temperature fit, the PSPC spectra of NGC 4365 and NGC 4382 have high temperature components with $kT > (1.0$–1.5) keV and $L_X \sim$ a few 10^{40} ergs s^{-1} (see Tables 3 and 4). Because of its limited passband at the high energies, *ROSAT* cannot determine the temperature of the hard component accurately. However, the hardness and luminosity of this emission are consistent with those of spiral galaxies of similar optical luminosity, and in particular with those of bulge-dominated early-type spirals. The nearest example of

TABLE 4
FLUXES AND LUMINOSITIES IN THE 0.1–2.0 keV RANGE

GALAXY (NGC)	TWO-COMPONENT MODEL		SOFT COMPONENT		HARD COMPONENT	
	f_X^{a} (ergs cm^{-2} s^{-1})	L_X^{a} (ergs s^{-1})	f_X (ergs cm^{-2} s^{-1})	L_X (ergs s^{-1})	f_X (ergs cm^{-2} s^{-1})	L_X (ergs s^{-1})
4365.........	6.4×10^{-13}	5.6×10^{40}	3.2×10^{-13}	2.8×10^{40}	3.3×10^{-13}	2.9×10^{40}
4382.........	7.3×10^{-13}	6.4×10^{40}	4.7×10^{-13}	4.1×10^{40}	2.5×10^{-13}	2.2×10^{40}

[a] Unabsorbed values, assuming log N_H from Table 3. Statistical errors are 6.5% and 7% for NGC 4365 and NGC 4382, respectively. However, the error is dominated by the uncertainties in the spectral parameters (see text).
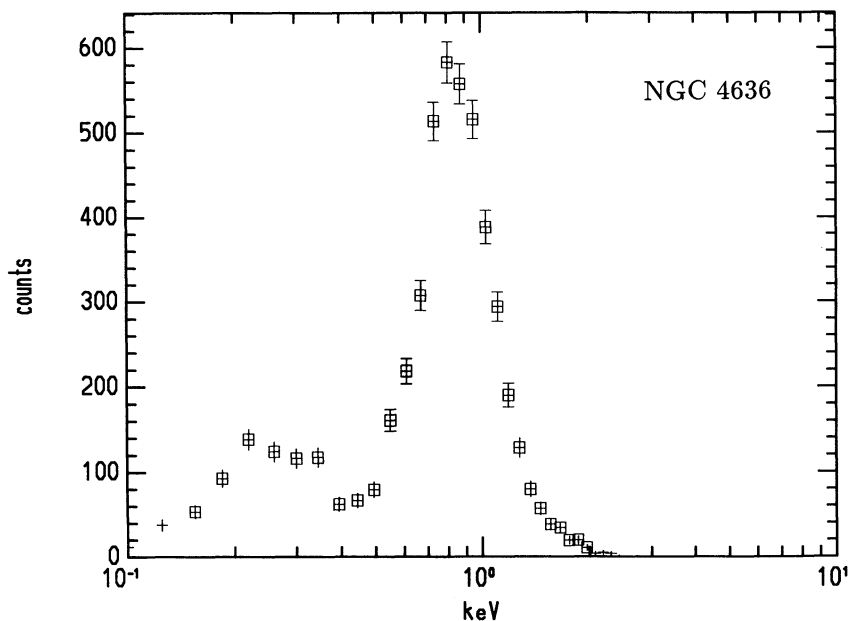
FIG. 9.—Observed distribution of the PSPC spectral counts of the X-ray–bright elliptical NGC 4636 (from Trinchieri et al. 1994)

these bulges, the bulge of M31, is dominated in X-rays by a population of pointlike sources, most likely low-mass binaries, and has a similar X-ray-to-optical ratio (Trinchieri & Fabbiano 1985, 1991; Fabbiano et al. 1987; Primini, Forman, & Jones 1993). This supports the suggestion that the hard component may be due to the integrated emission of a population of low-mass X-ray binaries, similar to those present in spiral bulges. These sources should be present in elliptical and S0 galaxies, which have a stellar composition similar to that of the bulges of early-type spirals (Kim et al. 1992b; Fabbiano 1989, and references therein; see Trinchieri & Fabbiano 1985 for the first detailed discussion of this point).

3.3. *The Soft Component*

The origin of the soft component is less clear. One possibility is that this emission originates also from the stellar population. This should be the case if these galaxies are stripped of their ISM by winds (see Ciotti et al. 1991) or by interaction with the cluster medium (e.g., White & Sarazin 1991). Kim et al. (1992b) suggested the possibility that this component is the integrated emission of the M star population in the galaxies. We really don't know anything about the X-ray emission of M stars outside the solar neighborhood, where these stars can be individually detected in X-rays (Schmitt et al. 1990; Barbera et al. 1993). To account for a few 10^{40} ergs s^{-1} we would need of the order 10^{12-13} M stars emitting $\sim 10^{27-28}$ ergs s^{-1} each. More detailed considerations, taking into account the possible shape of the IMF in these galaxies, and an age effect which seems to reduce the L_X of M stars in the solar neighborhood (Barbera et al. 1993), suggest that late-type stars may not account for the entire low-energy emission (Pellegrini & Fabbiano 1994). It is also possible, but very speculative at this point, that these galaxies contain a number of relatively bright very soft X-ray sources. Some of these sources have been reported in M31 (J. Trümper 1992, private communication). It would be interesting to look at the results of a full analysis of the observations of the bulge of M31, and compare the results with what we see in X-ray faint ellipticals. Pellegrini & Fabbiano (1994) specu-

late that supersoft sources, if present in elliptical galaxies, may be progenitors of SN Ia. A third category of stellar sources, with suitable soft spectral component are RS CVn systems (Dempsey et al. 1993). Their contribution to the soft component of X-ray faint early-type galaxies is found by Pellegrini & Fabbiano (1994; see companion paper) to be potentially important.

Another possibility is that these galaxies have not been stripped of their ISM, and that the very soft emission is due to an ISM at lower temperatures than seen in X-ray bright galaxies. This possibility is explored fully by Pellegrini & Fabbiano (1994), in the context of the D'Ercole et al. (1990) and Ciotti et al. (1991) evolutionary models of the ISM of early-type galaxies. The results of the *ROSAT* observations of NGC 4365, presented in this paper (L_X, PSPC spectral count distribution, surface brightness profile), are there used to constrain model parameters, together with the optical characteristics of this galaxy (stellar velocity dispersion, surface brightness profile). The result of this exercise suggests that the X-ray emission of NGC 4365 could be explained by a combination of a hard low-mass X-ray binary component, a very soft component of stellar origin, and a hot ISM component. The latter would be required to fit the shape of the X-ray surface brightness profile, which could be more extended than that of the optical light distribution. The hot ISM models that agreed more closely with the data imply a SN Ia rate ~ 0.6 of the Tamman rate, and an extended dark halo, with dark/luminous mass ratio ~ 9. Given the quality of the present data, this result is certainly not unique (see Pellegrini & Fabbiano 1994); however, it demonstrates the need of accurate good resolution spectral and spatial measurements of these galaxies in the X-rays.

4. SUMMARY AND CONCLUSIONS

We have observed with the *ROSAT* PSPC the two X-ray faint early-type galaxies NGC 4365 and NGC 4382. We detect extended X-ray emission from both galaxies, with similar count rates (0.06 counts s^{-1}) in the 0.1–2.0 keV band,

corresponding to fluxes of $6-7 \times 10^{-13}$ ergs cm^{-2} s^{-1}, and luminosities of $5-6 \times 10^{40}$ ergs s^{-1}, for the best-fit two-temperature spectral parameters. The X-ray spectra are well fitted with two thermal components: an optically thin Raymond spectrum with solar abundances and a well constrained kT of ~ 0.2 keV; and a high temperature (either Raymond or bremsstrahlung) component with $kT > \sim 1$ keV respectively. Both components would contribute to the emitted flux by comparable amounts. Alternate models that also fit the data well are a one-temperature low-abundance Raymond model, or equivalently a bremsstrahlung model with $kT \sim 0.6-1.1$ keV. The very tight constraints on the abundance in the case of NGC 4365, which was detected with a higher signal to noise ratio, led us to exclude the single Raymond model on the grounds of physical plausibility. The single bremsstrahlung model could be retained only by postulating a new class of X-ray emitting sources belonging to the stellar population. Given the present evidence, we adopt the two-temperature model as a more reasonable representation of the data.

These results confirm the earlier report of Kim et al. (1992b), who found differences in the average *Einstein* IPC spectra of early-type galaxies of different X-ray to optical ratios. In particular it is clear that the X-ray emission of X-ray faint elliptical galaxies is not due solely to the same type of hot ISM present in X-ray bright ellipticals.

We follow Kim et al. (1992b) in suggesting that the most plausible origin of the hard spectral component is the integrated emission of a population of low-mass X-ray binaries, similar to those responsible for the bulge emission of early-type spirals (see Fabbiano 1989). Several candidates exist for the very soft component. They include coronal emission of late-type stars, an unknown population of supersoft X-ray sources, and a hot/warm ISM. These are discussed in detail in the companion paper (Pellegrini & Fabbiano 1994).

These results demonstrate the importance of spectral data, supported by imaging, as a diagnostic of the X-ray emission properties and physical status of early-type galaxies. We hope to be able to explore more of the L_X/L_B plane of E and S0 galaxies with *ROSAT* and other X-ray satellites, to extend these studies and gather a more complete picture of the evolution of the ISM in these systems. In particular, observations with ASCA will remove the uncertainty on the spectral model that cannot be resolved with the present data, and will establish the presence (or less) of a hard emission component from low-mass binaries. *ROSAT* HRI observations will give us measurements of the surface brightness distribution which will help discriminating between gaseous ISM and stellar models. However, only with the spatial/spectral resolution of AXAF will we be able to investigate radial spectral variations that may give direct evidence supporting the suggestion of an extended hot/warm ISM.

REFERENCES

Barbera, M., Micela, G., Sciortino, S., Vaiana, G., Harnden, F. R., & Rosner, R. 1993, ApJ, 414, 846
Canizares, C. R., Fabbiano, G., & Trinchieri, G. 1987, ApJ, 312, 503
Ciotti, L., D'Ercole, A., Pellegrini, S., & Renzini, A. 1991, ApJ, 376, 380
David, L. P., Forman, W., & Jones, C. 1991, ApJ, 369, 121
Dempsey, R. C., Linsky, J. L., Schmitt, J. H. M. M., & Fleming, T. A. 1993, ApJ, 413, 333
D'Ercole, A., Ciotti, L., Pellegrini, S., & Renzini, A. 1989, ApJ, 341, L9
Fabbiano, G. 1989, ARA&A, 27, 87
———. 1993, in Structure, Dynamics, and Chemical Evolution of Elliptical Galaxies, ed. I. J. Danziger, W. W. Zeilinger, & K. Kjär (ESO Proc. No. 45), 617
Fabbiano, G., Gioia, I. M., & Trinchieri, G. 1989, ApJ, 347, 127
Fabbiano, G., Kim, D.-W., & Trinchieri, G. 1992, ApJS, 80, 531
Fabbiano, G., Trinchieri, G., & Van Speybroeck, L. 1987, ApJ, 316, 127
Forman, W., Jones, C., & Tucker, W. 1985, ApJ, 293, 102
Giacconi, et al. 1979, ApJ, 230, 540
Hasinger, G., Turner, J. T., George, I. A., & Boese, G. 1992, OGIP Calibration Memo CAL/ROS/92-001 (Greenbelt: NASA-GSFC)
Jones, C. 1977, ApJ, 214, 856
Kim, D.-W., Fabbiano, G., & Trinchieri, G. 1992a, ApJS, 80, 645
———. 1992b, ApJ, 393, 134
King, I. 1978, ApJ, 222, 1
Makishima, K., & Mitsuda, K. 1985, in Galactic and Extragalactic Compact X-ray Sources, ed. Y. Tanaka & W. H. G. Lewin (Tokyo: ISAS)

Morrison, R., & McCammon, D. 1983, ApJ, 270, 119
Pellegrini, S., & Fabbiano, G. 1994, ApJ, in press
Pfeffermann, E., et al. 1987, Proc. SPIE, 733, 519
Primini, F. A., Forman, W., & Jones, C. 1993, ApJ, 410, 615
Raymond, J. C., & Smith, B. W. 1977, ApJS, 35, 419
Renzini, A., Ciotti, L., D'Ercole, A., & Pellegrini, S. 1993, ApJ, 419, 52
Schmitt, J., Collura, A., Sciortino, S., Vaiana, G., Harnden, F. R., & Rosner, R. 1990, ApJ, 365, 704
Schweizer, F. 1993, in Structure, Dynamics, and Chemical Evolution of Elliptical Galaxies, ed. I. J. Danziger, W. W. Zeilinger, & K. Kjär (ESO Proc. No. 45), 651
Serlemitsos, P., et al. 1994, ApJ, in press
Stark, A., et al. 1992, ApJS, 79, 77
Surma, P. 1993, in Structure, Dynamics, and Chemical Evolution of Elliptical Galaxies, ed. I. J. Danziger, W. W. Zeilinger, & K. Kjär (ESO Proc. No. 45), 669
Trinchieri, G., & Fabbiano, G. 1985, ApJ, 296, 447
———. 1991, ApJ, 382, 82
Trinchieri, G., Fabbiano, G., & Canizares, C. R. 1986, ApJ, 310, 637
Trinchieri, G., Kim, D.-W., Fabbiano, G., & Canizares, C. R. 1994, ApJ, 428, 555
Trümper, J. 1983, Adv. Space Res., 2, No. 4, 241
Vaiana, G. 1990, in Imaging X-ray Astronomy, ed. M. Elvis (Cambridge: Univ. Press), 61
White, E. W. III, & Sarazin, C. L. 1991, ApJ, 367, 476